EUROPEAN ORGANIZATION FOR NUCLEAR RESEARCH

NOT TO BE CIRCULATED

8 March, 1966

P R O P O S A L

TO STUDY

LARGE MOMENTUM TRANSFER SCATTERING

W.F. Baker, P.J. Carlson, F. Krienen, A. Lundby,
R. Nierhaus, K. Pretzl*), and J.N. Woulds.

We would like to measure the angular distribution of π mesons elastically scattered from protons at large angles up to 180° and in the momentum range from 4 to 20 GeV/c. Simultaneously we can investigate certain inelastic processes at high momentum transfers.

For the experiment we intend to use a digitized wire spark chamber system with on-line computer. This would be placed in a high-intensity, high-energy, secondary pion beam produced by the slow extracted proton beam from the proton synchrotron.

The only process which has as yet been thoroughly surveyed up to the maximum momentum transfer possible is proton-proton elastic scattering.

1. PROCESSES TO BE STUDIED

1.1 Elastic scattering

The primary objective of this experiment is a full investigation of $\pi^+ + p$ and $\pi^- + p$ elastic scattering at large momentum transfers up to the highest energies possible with present-day accelerators and techniques. The items of greatest experimental interest are:

*) Visitor from Universität München.

a) the region near the tail of the forward diffraction peak where a persistent secondary maximum has been observed;

b) the intermediate-angle range where a behaviour characteristic of a statistical model might be expected;

c) the backward, or 180° region where the observed peaks indicate the dominance of baryon exchange.

For identical particles the maximum detectable scattering angle is 90° in the centre-of-mass, thus the largest momentum transfer measured in proton-proton scattering was $-t \simeq 24.4$ $(GeV/c)^2$ at an incident momentum of 30.9 GeV/c [1]. For πp scattering this momentum transfer is exceeded already at an incident momentum of 14 GeV/c.

Although the forward diffraction peak in πp elastic scattering has been quite thoroughly investigated, only a few points have been examined at larger angles. Full angular distributions have only been made at lower energies: for example, at 3.5 GeV/c by this group at CERN [2]. The region a) above has been examined at 8 and 12 GeV/c at Brookhaven and even at such relatively small momentum transfers the πp angular distribution is seen to deviate from the pp, not only in slope but also in magnitude (by a factor of ten or more) [3]. It is in this region also that the secondary maximum observed at lower energies is seen to persist at $-t \cong 1.3$ $(GeV/c)^2$. A similar effect has been seen in πp charge exchange and in Kp scattering.

The πp cross-section in the intermediate region between the forward and backward peaks, b) above, is so small that scattering in this range has until now essentially escaped detection at momenta above 4 GeV/c. It appears that the πp cross-sections lie well below the pp cross-sections.

Huang [4] has recently proposed an incoherent droplet model for high-energy scattering of strongly interacting particles in this angular region. He predicts an elastic cross-section of the form:

$$\frac{d\sigma}{d\omega} = A \exp[-\alpha P \sin \vartheta] ,$$

where P is the centre-of-mass momentum and α is a constant. This form is in agreement with the proton-proton scattering data[1,5], which give $A \cong 30$ mb/sr and $\alpha^{-1} \cong 152$ MeV/c. All that is now known about the pion-proton scattering cross-sections is that they appear to be smaller than the proton-proton cross-sections.

Evidence for a peak at 180° was first seen in $\pi^+ p$ scattering at 4 GeV/c[6], and peaks have subsequently been observed at several momenta for both $\pi^+ p$ and $\pi^- p$ scattering[2,3,7]; but the true character of these peaks remains to be determined. If in analogy with the forward peak we write for the backward peak the form

$$\frac{d\sigma}{dt} = \left(\frac{d\sigma}{dt}\right)_{180^{\circ}} \cdot \exp\left[\alpha \left| t_{180^{\circ}} - t \right|\right]$$

then it appears that several conclusions can be drawn from the data.

i) The cross-section at 180° for $\pi^+ p$ scattering is about five times the $\pi^- p$ cross-section.

ii) The cross-section at 180° has an energy dependence of the form $s^{-1.5}$, where s is the centre-of-mass energy squared.

iii) The $\pi^+ p$ cross-section at 180° is down by a factor of 300 from the 0° value at 3.5 GeV/c.

iv) The slope, α, is comparable to that of the forward diffraction peak.

The importance of a precise measurement of the backward peaks as a test for Regge behaviour has been discussed by Chew and Stack[8]. As backward $\pi^- p$ scattering is predominantly attributable to one trajectory, the Δ, Regge theory predicts a shrinkage (change in slope) of 50% when the momentum is raised from 4 to 20 GeV/c.

Heinz and Ross have pointed out the advantages of determining the spins of pion-nucleon resonances by scattering in the backward direction[9]. They have also suggested that new resonances

could be discovered by this technique over a mass range twice as large as has already been explored. The attempt to find higher resonances as bumps in the total cross-section distribution becomes more difficult at higher energies as more inelastic channels open up to compete with a resonance. Unlike the total cross-section, the 180° elastic cross-section drops off with energy and the competition should not be as severe. If the resonant amplitude interferes coherently with an assumed baryon exchange "background" amplitude, then there will be a large modulation in the energy distribution of the backward differential cross-section as the centre-of-mass energy passes through the resonance. With the success of this technique one can learn if the baryon mass spectrum continues on upward or if it terminates.

An experiment[10] has just been completed at the Argonne Laboratory in which the differential cross-section for $\pi^- + p$ elastic scattering at 180° was measured in small steps from 1.6 to 5.3 GeV/c. This corresponds to centre-of-mass energies of 1975 to 3300 MeV. The cross-section shows considerable structure which is attributed to various nucleon resonances. In addition to the known resonances, a new one is seen with a mass of 3245 ± 10 MeV.

These new results provide strong motivation for continuing the search with this technique up to the higher energies possible at the CERN PS. The mass range can be extended up to 6000 MeV. In addition, because of CERN's unique ability to provide counter beams from an external target, the same search can also be made in $\pi^+ + p$ scattering. In this case only the $I = 3/2$ resonances can appear, and the cleanest results can be obtained.

1.2 Inelastic processes

The equipment of this experiment is specifically designed to study elastic scatterings (Fig. 1), and as such it measures the angles and momenta of two outgoing charged particles. However, one can simultaneously measure any process for which the kinematical

relationships are sufficiently similar to those for elastic scattering. At large momentum transfers these relationships are particularly favourable.

1.2.1 Nucleon resonances

Most similar to elastic scattering is the production of a nucleon resonance which then decays into a neutral pion and a proton:

$$\pi^{\pm} + p \rightarrow \pi^{\pm} + N^{*} \hookrightarrow \pi^{0} + p \ .$$

When a large momentum is imparted to the resonant particle, the decay proton is emitted in a small cone about its direction. The pion cone angle is considerably larger. A comparison of $N^{*}(1236)$ production and decay with elastic scattering at an incident momentum of 6.0 GeV/c is given in Fig. 2. The limits of the angular and momentum ranges of the decay protons are given by the dashed lines. These ranges lie within the acceptance of the apparatus when it is set for elastic scattering above 30°. At higher incident momenta the ranges become even smaller and nearer to elastic. On the other hand, a resonance of larger mass will have larger ranges of proton angles and momenta. Figure 3 shows the $N^{*}(2190)$ at 16.0 GeV/c. If the angular distribution of the decay of the resonance is known, then there will be no threshold imposed by the aperture of the apparatus. In any case, the s and t dependence of nucleon resonance production can be measured with no increase in running time.

1.2.2 Associated production

Only slightly more difficult topologically is the process

$$\pi^{+} + p \rightarrow K^{+} + \Sigma^{+} \hookrightarrow \pi^{0} + p$$

because the Σ has a relatively short decay length. The relevant kinematical relations are given in Fig. 4 for 6.0 GeV/c.

2. EXPERIMENTAL EQUIPMENT

The various components for this experiment have been chosen to match each other and to form an integrated system with a data-taking rate at least an order of magnitude greater than systems of comparable resolution now in use at CERN. Nearly all of the elements are newly constructed. The basic logic, however, is identical to our previous experiment at lower energies; specifically, it is to measure the momenta and directions of all particles involved in the reaction. To do this three spectrometers are used: one short resolving-time spectrometer for the incident particle, and two large-aperture spectrometers for the outgoing particles. The detectors are to be connected directly to a computer for immediate analysis of the events.

The two large-aperture spectrometers use wire spark chambers with a ferrite core read-out system; these were the starting point in developing the apparatus for the experiment. To utilize the high data-rate capability of these chambers some other experimental techniques are also being developed. In particular, an intense beam has been designed using the slow-extracted proton beam from the PS.

2.1 The high intensity beam

The existing high-energy pion beams at the PS are limited in intensity by the small angular acceptance that is obtained from an internal target and, particularly for positive particles, by the fact that the fringing field prevents catching the particles produced in the peak at a production angle of 0°. These problems are overcome when the production target is placed in the extracted proton beam external to the PS ring. However, one then loses the multiple traversals which take place in an internal target. This loss can, to a large extent, be overcome with a sufficiently thick target. A thick target does not seriously harm the optical properties of the following secondary beam, as it is viewed at 0°. The net gain over

the existing "d" beams is calculated to be about a factor of ten for negative pions and about a factor of one hundred for positive pions. Because of the shorter beam length, the gain for kaons should be even greater. The expected pion intensities[11] are given by Fig. 5.

The ray diagram in Fig. 6 shows the focusing characteristics of the beam proposed for this experiment[12]. It can transport particles up to 20 GeV/c and has a comparatively short length, 49 metres. The first section, up to the momentum slit, is not unusual, except that no vertical focus is produced at the slit. The dipole magnet D1 is a septum bending magnet through which both the secondary and primary beams pass. Only the secondary beam is collected by the split-pole quadrupole magnet Q_1, which together with Q2 and Q3 forms a symmetric triplet. D2 disperses the beam at the momentum slit for momentum selection.

The second half of the beam is primarily a spectrometer for momentum analysis of the incident particles. Vertically, the beam is simply focused on the hydrogen target. In the horizontal plane the system is symmetric about the horizontally focusing quadrupole Q4, which focuses the plane of the momentum slit onto the plane of the hydrogen target. The dipoles D_3 and D_4 overly recombine the momentum such that the dispersion at the hydrogen target is equal to the dispersion at the momentum slit, which is 5 mm/per cent momentum interval. Counter hodoscopes placed in these two positions form the spectrometer, since a particle of a given momentum passing through a given counter in the first hodoscope must strike a unique counter in the final hodoscope independent of the path followed. There is some redundancy in this system in that the dispersion at the momentum slit permits some momentum determination by that hodoscope alone.

The resolution of this technique is limited by the "chromatic" aberration as well as the finite size of the hodoscope elements. This aberration increases linearly with distance from the median

momentum P_0. For example, at ± 1% from P_0, the limit of resolution is calculated to be ± ⅛%, and at ± 2% to be ± ¼%.

Because of the "chromatic" aberration, the image size at the hydrogen target is not small: 2.5 cm horizontally by 5 cm vertically for a momentum acceptance of ± 2%. This is intentional and helps in distinguishing simultaneously incident particles. The size can be reduced by a factor of two in each dimension by halving the momentum acceptance.

2.2 The triggering logic

The requirements for triggering the spark chambers are kept as general as possible in order to introduce a minimum of biases into the experiment. This leads to a comparatively high trigger rate and is only possible because of the relatively high frequency at which a wire chamber system can operate. A relaxed triggering requirement is also necessary because several different processes are studied simultaneously.

The incident particle telescope is of the usual type with threshold gas Čerenkov counters[13] to identify the incident particle. It is independent of the hodoscopes. The segmented counters S_4 and S_5 (Fig. 1) indicate when one particle is emitted into the forward hemisphere and one is emitted into the backward hemisphere (centre-of-mass).

The downstream Čerenkov counter is of critical importance in studying large momentum transfer reactions. It is a threshold counter set to count the incident beam particles, pions in this case, and connected in anticoincidence with the rest of the triggering logic. This is necessary to suppress the small momentum transfer events which are orders of magnitude more frequent than the large-angle reactions. A schematic drawing of this counter is shown in Fig. 7. It was specifically designed to have a large aperture to match the wire chambers and the magnet preceding it. It is to operate with freon gas at atmospheric pressure. With freon-114

the threshold momenta for pions, kaons and protons are 2.7, 9.5 and 18 GeV/c, respectively, and with freon-22 they are 3.6 12.8 and 24 GeV/c, respectively. An adjustable "black" pipe through the counter will permit the incident beam to pass without overloading the electronics.

2.3 The wire spark chambers

The digitized planes are wound of 0.1 mm diameter phosphor-bronze wire with a spacing of 1.25 mm on glass frames. Both the high-voltage plane and the ground plane are made this way, and they are separated by a gap of 3.8 mm. A novel feature in these chambers is the crinkling of the wires which keeps them taut with relatively little tension. A chamber consists of one X gap and one Y gap and is filled with argon gas plus an organic quencher. Including the plastic walls, each chamber has an average thickness of 30 milligrams per square centimetre.

The chambers are driven with double spark gap pulsers which initiate and terminate the chamber discharge. Each wire of the high-voltage plane is fed through a series resistor. Each wire of the ground plane passes through a ferrite core which is flipped by the current of the discharge. These are in turn read by the electronic read-out system, and the contents are stored in the memory of a computer.

The two chamber sizes are: "A" chambers: 96 cm horizontally by 48 cm vertically (768 by 384 wires); and "B" chambers: 128 cm by 64 cm (1024 by 512 wires).

2.4 The two large-aperture spectrometers

Two magnetic spectrometers incorporating the wire chambers are used to measure the angle and momentum of each of the two charged particles leaving the hydrogen target (Fig.1).

Two large-aperture C-magnets have been specially designed[14] and a photograph of them is shown in Fig. 8. They are identical in construction, and each has a pole-tip area 1 metre by 1 metre and

a 50 cm high gap. The integrated bending power of each is approximately 20 kilogauss-metres. The yokes are asymmetric to permit the magnets to fit in the experimental area without excavation and, at the same time, to fit snugly around the hydrogen target.

Each spectrometer contains four "A" chambers before the magnet and two "B" chambers after it. This provides for complete redundancy in that only two "A" chambers and one "B" chamber need operate to establish the direction and momentum of a particle.

2.5 The hodoscopes

With the expected incident fluxes of about 10^7 particles in a 100 millisecond burst from the PS, spark chambers, which have a resolving time of approximately 1 microsecond, would be overloaded. We therefore intend to use small scintillation counter hodoscopes to measure the direction and momenta of the incident particles.

In principle, these hodoscopes are small area, fast resolving-time, wire chambers. That is, in the read-out and data-processing systems they are handled in the same way. The output signals from the photomultiplier tubes are sent, after a suitable delay, to a master fast gate of 5 nanoseconds width. This gate is opened by the trigger which fires the wire chambers. The pulses which pass the gate are used to flip ferrite cores. These cores are read in turn along with those of the wire chambers.

In addition to the chromatic aberration mentioned previously, the resolution of the incident beam spectrometer is limited by the width and thickness of the hodoscope elements. As the cost is proportional to the number of elements, and not their size, it is necessary to minimize this number for a given resolution and beam intensity. The focusing spectrometer described in section 2.1 seems optimum in that it requires only two hodoscope planes for momentum measurements.

In addition to these two small-element hodoscopes, three more are necessary to determine the direction of the incident particle. One of these, also with small elements, measures vertical position just before the hydrogen target. The remaining two, with larger elements, are placed just after the final bending magnet and complete the determination of direction in the horizontal and vertical planes.

2.6 The read-out system

An electronic read-out system[15] has been constructed which transfers the data to the on-line computer. This system interrogates the ferrite cores in groups of 32, and passes on the information to the computer in the form of track co-ordinates. It also contains some test features for examining the cores and the read-out system itself. The components are shown in the photograph of Fig. 9.

The time required by this unit to read out one event is determined by the number of groups of 32 to be interrogated plus the number of track co-ordinates to be transferred. The cycle time is 1 microsecond for each group of 32, and the time required to transfer one co-ordinate to an IBM 1800 computer is 4 microseconds. For a typical event, 1.0 to 1.5 milliseconds will be required. It now appears that it is this read-out time which limits the rate at which the chambers can be triggered.

2.7 The on-line computers

The advantages of immediate analysis of one's data are apparent to any experimentalist. A block diagram of the data reduction system is shown in Fig. 10. All detectors are connected, via the read-out system, to a small computer, IBM 1800, which in turn is connected via a data link to the CDC 6600.

The primary purpose of the local computer, 1800, is to collect all the data during one PS burst. Only a core memory is fast enough to do this. Of the 16K memory, 5K to 10K will be used for this purpose. The rest of the memory will hold short programmes

to monitor the operation of the spark chambers and to perform other control functions. Some simple filtering will be performed in the 1800 by checks on the consistency of the data, but otherwise no analysis will be done on the 1800 during the run. The filtered data will be recorded on magnetic tape between PS bursts and sent to the 6600 for analysis. As it will be operating under a time-sharing system, the 6600 may not be able to accept all the data at once, so it is intended to "play back" to the 6600 at a later time the data recorded by the 1800.

A more complete description of the data flow and analysis is given by the data flow diagram of Fig. 10 and the programme flow chart of Fig. 11. The 6600 programme is essentially the programme PEST which we are now using to analyse the spark-chamber photographs of our previous experiment.

3. RESOLUTION OF THE SYSTEM

Of the two types of background, unwanted (or inelastic) events and accidentals (or chance events), the latter only contributes to extraneous triggering of the chambers. The former must be rejected by kinematical analysis.

In general, the closest unwanted event to the desired event is the desired event plus the production of a neutral pion. This sets the spatial and momentum resolution required. (One cannot hope in an experiment like this to separate out events with "soft" gamma-ray production.)

3.1 Requirements

The combined errors in the system must not be greater than the pion mass. This is facilitated by measuring all parameters of the charged particles; these are the momentum of the incident particle and the momenta of two outgoing particles plus the angle of each with respect to the incident particle. For elastic scattering this is a twofold over-determination.

The rejection of inelastic events clearly becomes more difficult the higher the energy. In the high-energy limit (E = cP), the resolution requirement on the momentum measurements alone is given by conservation of energy with the production of a neutral pion at rest in the laboratory system:

$$\Delta P_o + \Delta P_\pi + \Delta P_p < m_{\pi^o} \ ,$$

where P_o, P_π and P_p are the momenta of the incident pion, the scattered pion, and the recoil proton, respectively.

For scattering into the backward hemisphere this relation is sufficient but not necessary. Here, the momentum of the elastically scattered pions, about 0.5 GeV/c, is not only quite insensitive to angle and incident energy, but it is greater than that of any inelastically scattered pion. It can be shown that all events which produce a neutral pion can be rejected if the momentum resolutions satisfy the relation

$$\Delta P_\pi \cdot \Delta P_p < \tfrac{1}{4} \, m_{\pi^o}^2$$

i.e.

$$\Delta P_\pi \cdot \Delta P_p < 4550 \ (\text{MeV/c})^2 \ .$$

In this region, accurate measurements of incident momenta and scattering angles are not helpful in eliminating inelastic background. The momentum requirement, however, is much less stringent than the previous relation above; for example, a 2% accuracy in measuring the pion necessitates only a 450 MeV/c accuracy in measuring the proton. This relation is significant, for it is the recoil protons from backward scattering that have the highest momentum we have to measure.

The necessary angular resolution can best be seen at intermediate angles where the effect of producing a pion at rest can be described by the following construction in which, to conserve

longitudinal momentum, the energy of the created pion is obtained by decreasing the transverse momenta of the charged secondaries.

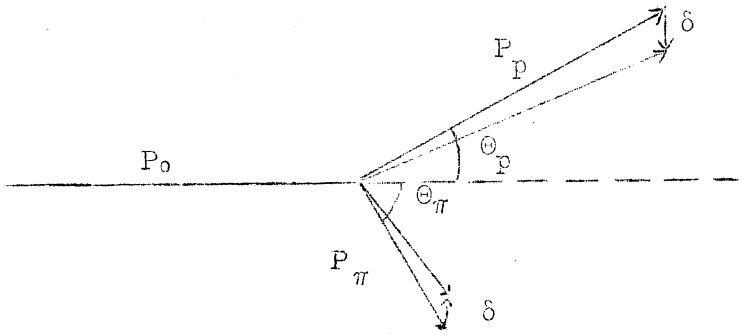

For each particle the angle changes by $\Delta\Theta \cong (\delta \cos \Theta)/P$ and the momentum by $\Delta P \cong \delta \sin \Theta$, where $\delta \cong m_\pi/(\sin \Theta_p + \sin \Theta_\pi)$. Thus, at some angles the momentum measurement best rejects inelastic events, and at other angles the angular measurement best rejects them. Typical numbers are given by the case of 90° scattering in the centre-of-mass at 20 GeV/c; these are $\Delta\Theta$ = 21 mr and ΔP = 70 MeV/c for each particle; note that only two of these four measurements are necessary to establish an elastic event.

3.2 Incident beam resolution

For a given bending angle the momentum resolution in the incident beam is set by multiple scattering, chromatic aberration, or the size of the hodoscope elements depending on the momentum and the momentum spread of the beam.

Coulomb scattering is determined by the 1 g/cm^2 of counters and hodoscopes in the beam. The 2 g/cm^2 of air is removed with helium bags. This error is essentially independent of momentum and is 25 MeV/c. As previously stated, the chromatic aberration with a momentum spread of ± 2% is ± ¼% or 50 MeV/c at 20 GeV/c. The width of the hodoscope elements, 3 mm, contributes a $\Delta P/P$ of ± ⅓% or 70 MeV/c at 20 GeV/c.

The angular resolution in measuring the incident beam is determined by the pairs of hodoscopes following the last dipole magnet and preceding the hydrogen target. The elements in the former are considerably larger than those in the latter, and together they produce an angular definition of ± 1.5 mr in both planes.

3.3 Resolution of the large aperture spectrometers

These spectrometers are adjustable in length as well as in position, and thereby their resolution is adapted to suit the particle being measured. The momentum and angular resolution are, in general, set by the wire spacing and the length of the spectrometer. For example, to analyse a 16 GeV/c particle the length would be set at 11 metres for 100 MeV/c resolution. The 30 mg/cm^2 thickness of the wire chambers is so small that it limits the momentum resolution only for the backward scattered pions. This limit is 10 MeV/c. Here, the spectrometer would be made as short as possible for maximum solid angle. Angular resolution in all cases would be better than ± 1 mr.

4. EXPECTED EVENTS RATE

The minimum detectable cross-section we estimate using a 1 metre liquid hydrogen target, a beam of 10^7 particles per burst (Fig. 5), a solid angle of 7×10^{-2} steradians, and require one count per hour. This yields:

$$\left(\frac{d\sigma}{d\omega}\right)_{lab} \geq 3 \times 10^{-33} \text{ cm}^2/\text{sr}.$$

To estimate the rates for elastic pion scattering at 180^0 we use the conclusions in Section 1.1 and obtain the values given in the table below. The background rates given are for the inelastic events which trigger the chambers. The most pessimistic assumption is

made: that the cross-section for inelastic events remains constant in the centre-of-mass with increasing energy and is equal to the result we obtained at 3.5 GeV/c.

	P_o (GeV/c)	$(d\sigma/d\omega)_{cm}$ (10^{-30} cm^2/sr) (estimated)	elastic events/ hour	inelastic events/ pulse	Limiting factor
π^+	6	25	453	50	Trigger rate
	10	11	41	10	Beam protons
	16	5	0.5	0.2	" "
π^-	6	5	59	13	Beam intensity
	10	2	21	10	"
	16	1	3	3	"

These rates are for a 12 cm hydrogen target, which is more suitable at 180^o. Besides insufficient beam intensity several factors can set the limit to the rate: an upper limit to the incident beam of 2×10^7 particles per pulse, in order not to overload the hodoscopes, limits the event rates for high-energy π^+ points where there is a large proton contamination, and a maximum of 100 spark-chamber triggers per pulse limits the low-energy points.

Our estimate of false triggers due to accidental (chance) coincidences in the triggering logic is based on our experience at 3.5 GeV/c. With a properly shielded system and collimated beam these should be due to two or more particles interacting in the target within the resolving time of the electronics. Extrapolating our previous results to the higher intensities of this experiment, predicts an accidental rate in each case lower than the inelastic rates of the table above. The real answer to this question, however, can only come from experience.

5. TIME SCHEDULE AND REQUIREMENTS

5.1 Schedule

At the time of writing this proposal the status of components for the experiment is as follows. Several of the wire spark chambers have been built and tested. The large C magnets have been delivered to CERN, and measurement of them should be completed in May, 1966. Construction of the electronic read-out system has been completed. The incident beam Čerenkov counters are under construction and should be completed by March, 1966. The large downstream Čerenkov counter is being designed in detail and could be completed in June, 1966. The hodoscopes also are being designed and could be ready in June, 1966. The IBM 1800 computer is scheduled for delivery in June, 1966 and, allowing a time for testing, should be available for use in August, 1966. Many of the programmes for the 1800 have been written and tested on the CDC 6600 using an 1800 simulator which we have written. As previously noted, most of the 6600 programmes required are now in use.

On the basis of this schedule we would be able to start testing the assembled system in a beam in September, 1966. We would be ready to start data-taking two months later.

5.2 The proposed experiment

On-line equipment such as this must first be extensively tested before the data-taking phase of the experiment can begin. In particular, the analysis programmes must be in reliable operation if the advantage of an on-line experiment is to be realized.

We intend dividing the experiment itself into three phases corresponding to the three angular regions described in Section 1.1.

1. We would first look in the small-angle region, 1.1 a), to investigate the energy dependence of the secondary maximum in the elastic scattering. The cross-sections should be large here,

and not too much time will be required. The high fraction of elastic events will help in finding any remaining flaws in the system.

2. In the second phase we would study the peaks at 180°, 1.1 c). We would measure their size and shape at several energies up to the maximum energy possible and expect to establish the existence or lack of shrinkage. We would then begin a systematic measurement of the 180° cross-section in small energy steps to search for "resonances" and continue it as long as it proves fruitful.

3. The final and most difficult region will be the intermediate angles, 1.1 b), where evidence indicates that the cross-sections are considerably smaller than in the previous two regions. At the completion of this programme the complete angular distribution should be known.

It is more difficult to predict angular distributions for the production of nucleon resonances, as little is known about them at large momentum transfers. However, it is not unreasonable to expect that we would obtain some knowledge of these distributions at no additional cost in running time.

5.3 Time requirements for the proposed experiment

1. For testing we require 100 shifts (two months) of PS time on a parasitic basis. This would be with the assembled system in its final position and with $1 - 2 \times 10^{10}$ protons per pulse on the external production target.

2. For the first two angular regions listed above we require 100 shifts with about 5×10^{11} protons per pulse on the production target. Additional time necessary to complete a "resonance" search would be requested at a later date.

3. The time required for region 3 can be better estimated when data is available from the first two.

5.4 Future measurements

It is clear that this system is well suited to other large momentum transfer experiments in addition to the one proposed here. In the future, we envisage proposing experiments to measure:

i) the scattering of K mesons and antiprotons for which beam separators will be advisable;

ii) spin dependences in large-angle scattering with the installation of a polarized target.

REFERENCES

1) W.F. Baker, E.W. Jenkins, A.L. Read, G. Cocconi, V.T. Cocconi, A.D. Krisch, J. Orear, R. Rubinstein, D.B. Scarl and B.T. Ulrich, Phys.Rev. Letters 12, 132 (1964).

2) A preliminary report on this work was presented at the Oxford International Conference on Elementary Particles, 19 - 25 September, 1965.

3) J. Orear, R. Rubinstein, D.B. Scarl, D.H. White, A.D. Krisch, W.R. Frisken, A.L. Read and H. Ruderman, Phys.Rev. Letters 15, 309 and 313 (1965).

4) K. Huang, Incoherent droplet model of high-energy large-angle scattering (preprint).

5) J. Orear, Phys.Rev. Letters 12, 112 (1964).

6) Aachen-Berlin-Birmingham-Bonn-Hamburg-London-München Collaboration, Physics Letters 10, 248 (1964).

7) J.A. Savin, A.S. Vovenko, B.N. Gus'kov, M.F. Likhachev, A.L. Lyubimov, J.A. Matulenko and V.S. Stavinsky, Physics Letters 10, 248 (1964) and Dubna Report P-2327 (1965).

8) G.F. Chew and J.D. Stack, UCRL-16293 (1965).

9) R. Heinz and M. Ross, Phys.Rev. Letters 14, 1091 (1965) and private communication.

10) S.W. Kormanyos, A.D. Krisch, J.R. O'Fallon, K. Ruddick and L.G. Ratner, private communication (to be published).

11) The data presented in the thesis of B. Jordan were used, CERN 65 - 14 (1965).

12) Designed by G. Petrucci.

13) M. Vivargent, G. von Dardel, R. Mermod, G. Weber and K. Winter, Nucl.Instr. and Methods 22, 165 (1963).

14) Designed by M. Morpurgo.

15) Designed by J. Lindsay and T. Pizer.

Figure Captions

Fig. 1 : Floor plan of the experiment.

Fig. 2 : Kinematics for the process $\pi + p \rightarrow \pi + N^*(1236)$ at 6 GeV/c.

Fig. 3 : Kinematics for the process $\pi + p \rightarrow \pi + N^*(2190)$ at 16 GeV/c.

Fig. 4 : Kinematics for the process $\pi + p \rightarrow K + \Sigma$ at 6 GeV/c.

Fig. 5 : Expected beam intensities from an external target.

Fig. 6 : Focusing properties of the high-energy secondary beam.

Fig. 7 : Downstream Čerenkov counter.

Fig. 8 : Photograph of C-magnets.

Fig. 9 : Photograph of read-out system.

Fig. 10 : Data flow diagram.

Fig. 11 : Programme flow chart.

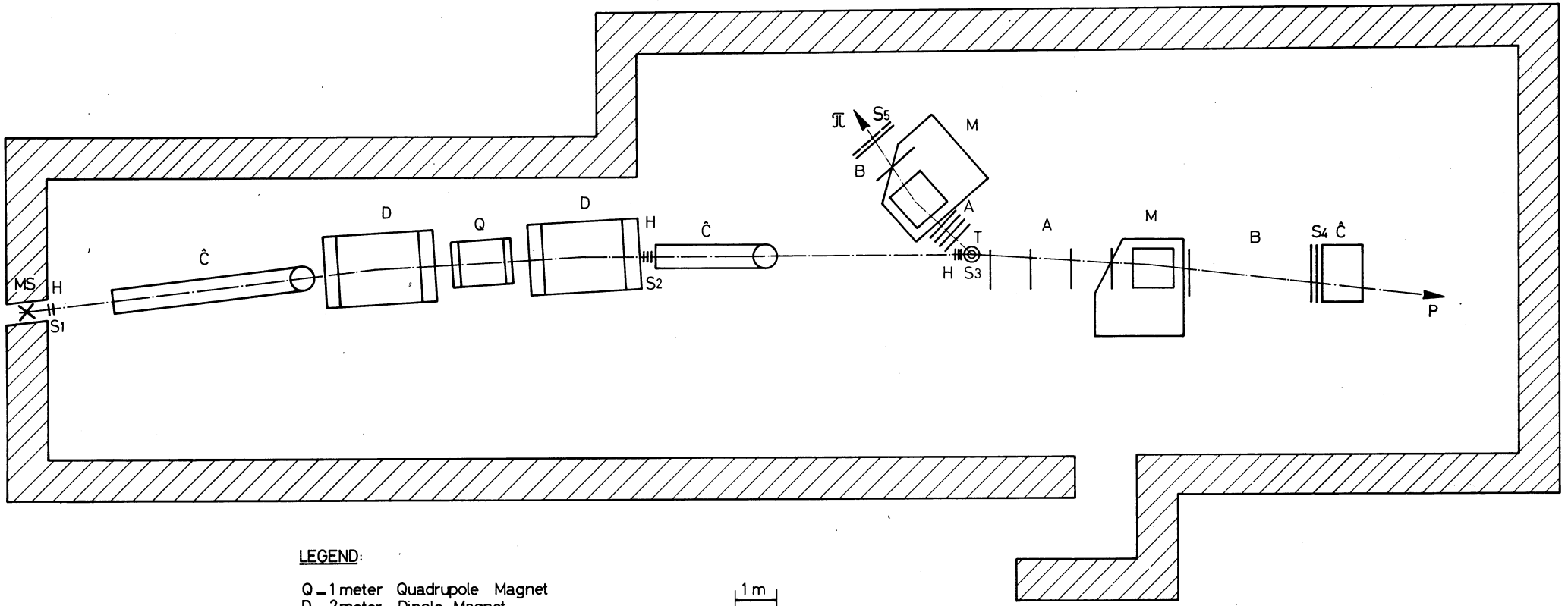

LEGEND:

Q = 1 meter Quadrupole Magnet
D = 2 meter Dipole Magnet
M = 1x1x0.5 meter^3 C-Magnet
Ĉ = Threshold Čerenkov Counter
S = Scintillation Counter
H = Scintillation Counter Hodoscope
B = 1.28x0.64 m^2 Wire Chamber
A = 0.96 x 0.48 m^2 Wire Chamber
T = 12 or 100 cm Hydrogen Target
MS = Momentum Slit

Fig.1 LARGE MOMENTUM TRANSFER EXPERIMENT

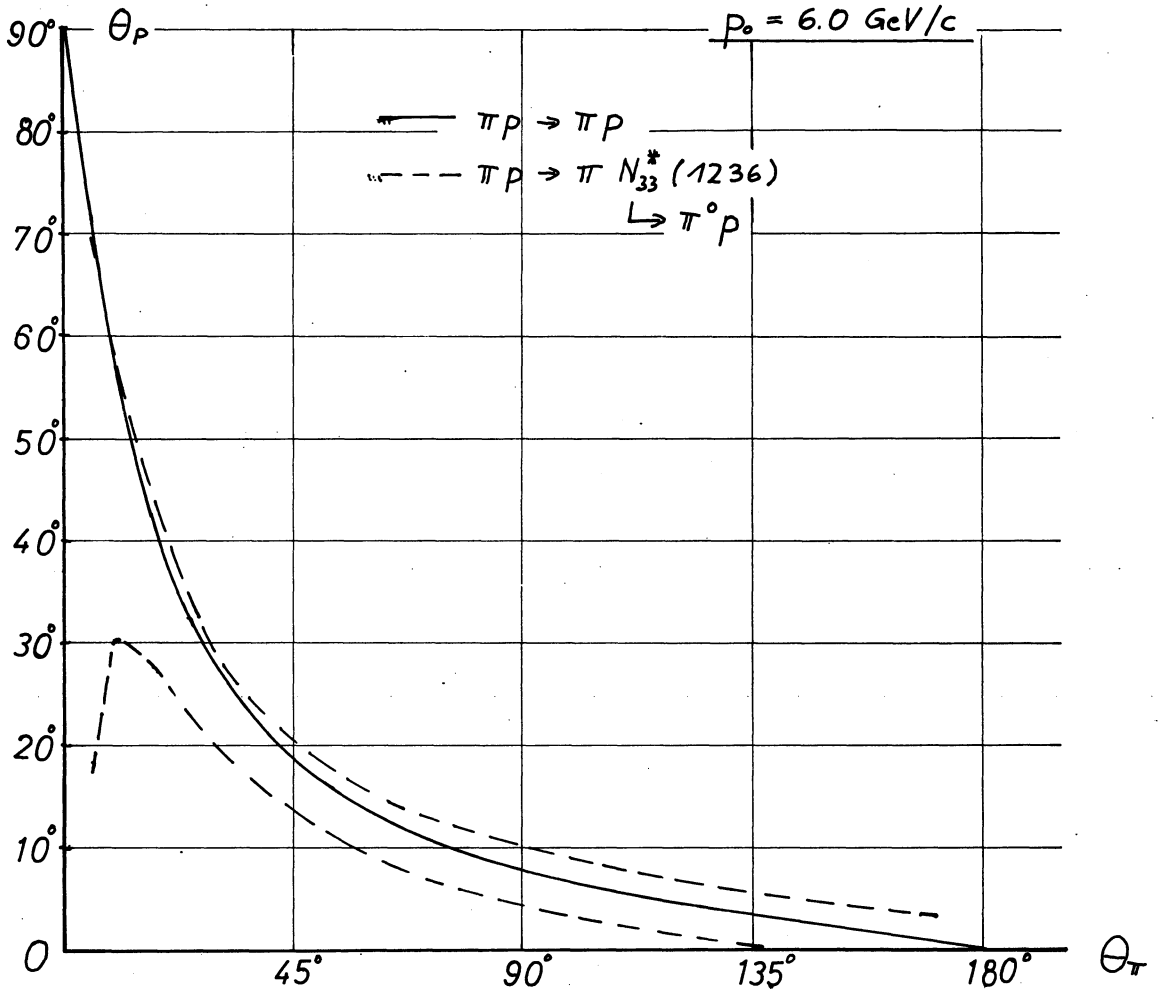
θ_p
p_o = 6.0 GeV/c
$\pi p \to \pi p$
$\pi p \to \pi N_{33}^{*}(1236)$
$\hookrightarrow \pi^{\circ} p$
90°
80°
70°
60°
50°
40°
30°
20°
10°
0
45°
90°
135°
180°
θ_π

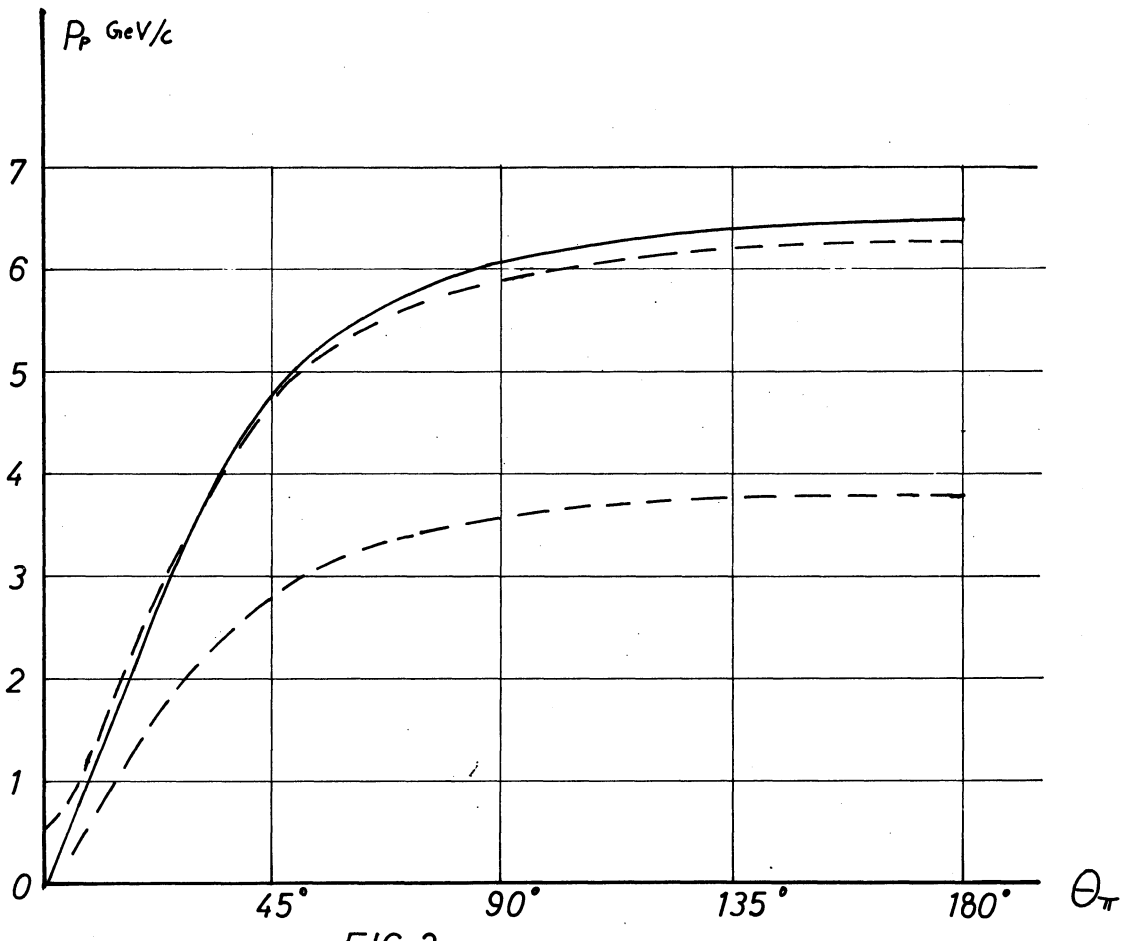
P_p GeV/c
7
6
5
4
3
2
1
0
45°
90°
135°
180°
θ_π

FIG. 2

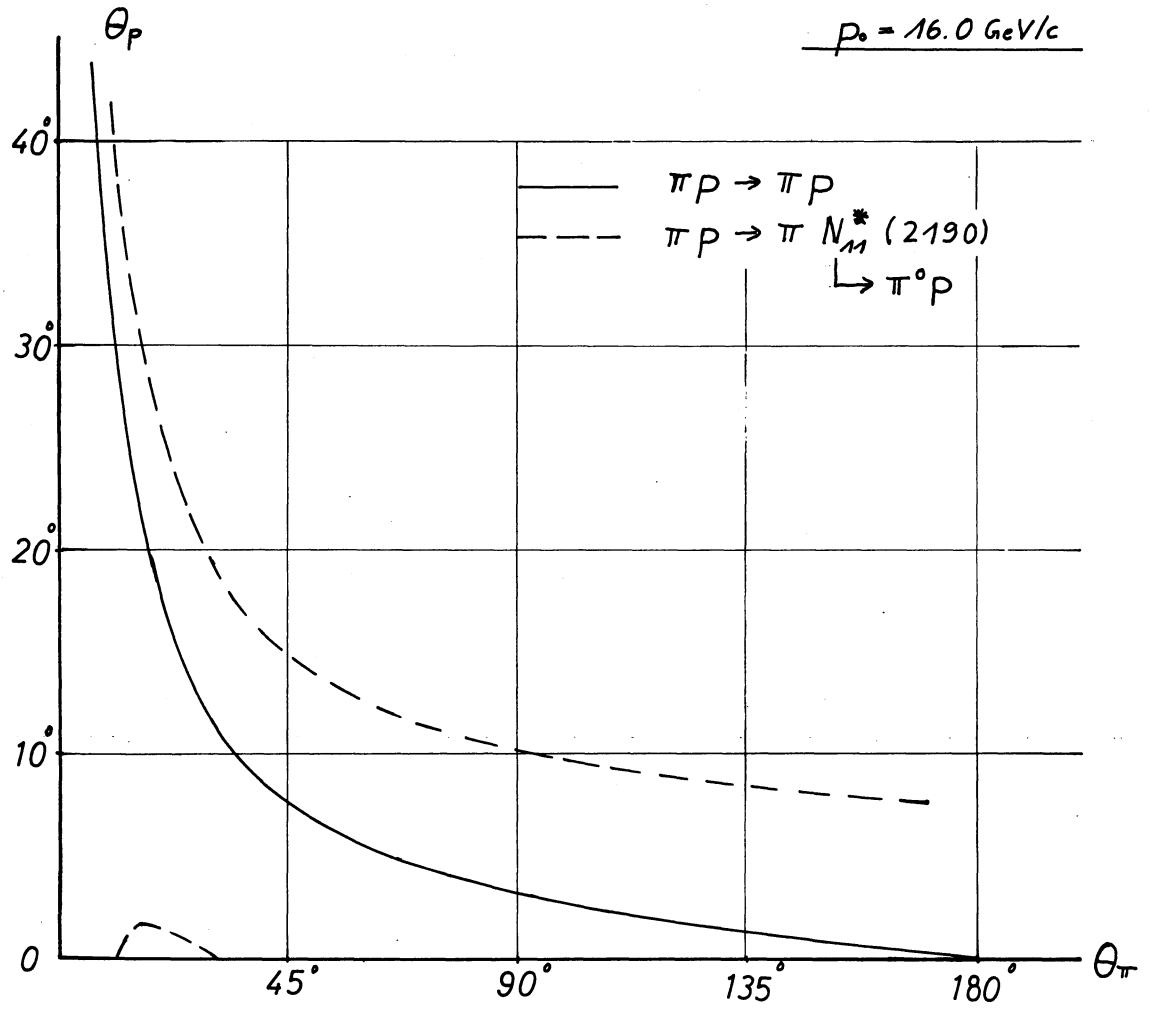
θ_p
$p_0 = 16.0$ GeV/c
40°
30°
20°
10°
0
$\pi p \to \pi p$
$\pi p \to \pi N^*_{11}(2190)$
$\hookrightarrow \pi^0 p$
45°
90°
135°
180°
θ_π

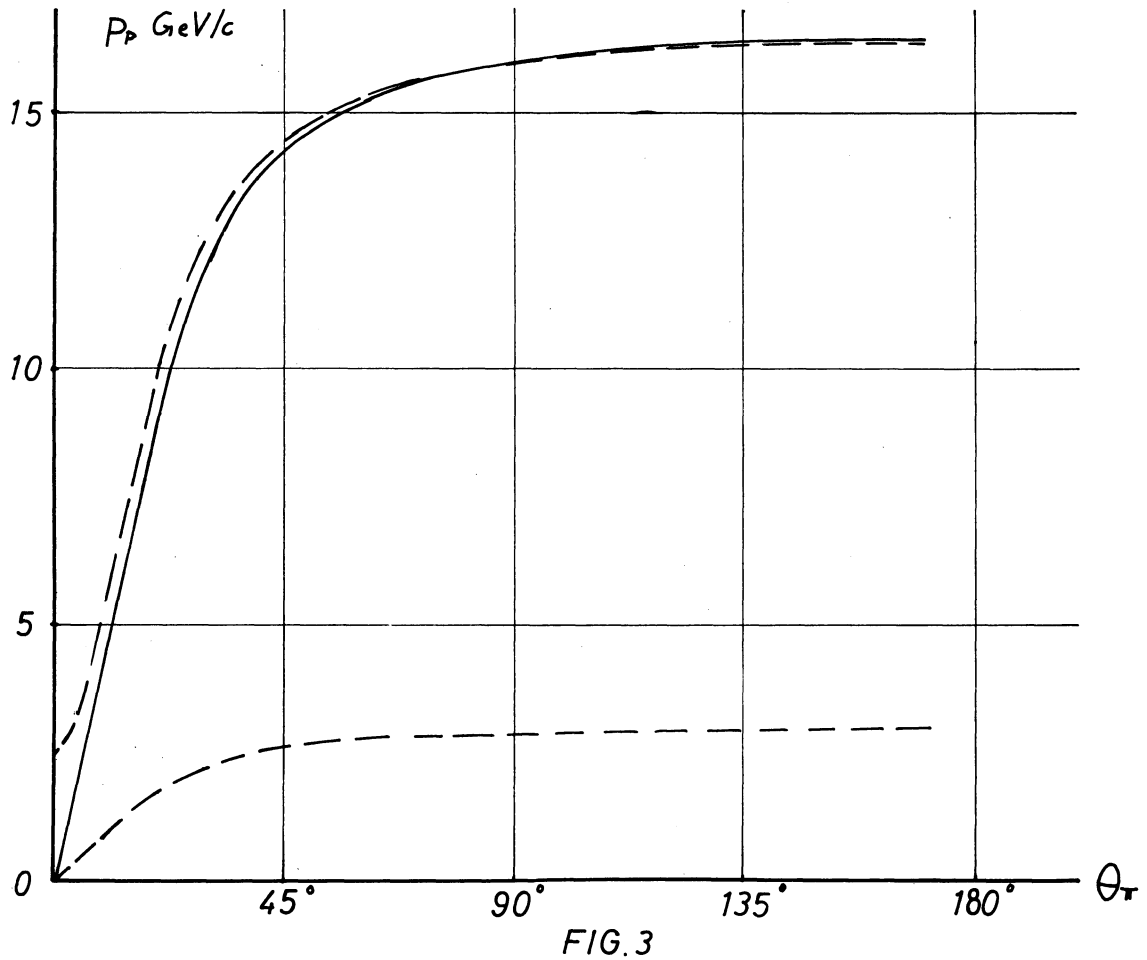
P_p GeV/c
15
10
5
0
45°
90°
135°
180°
θ_π

FIG. 3

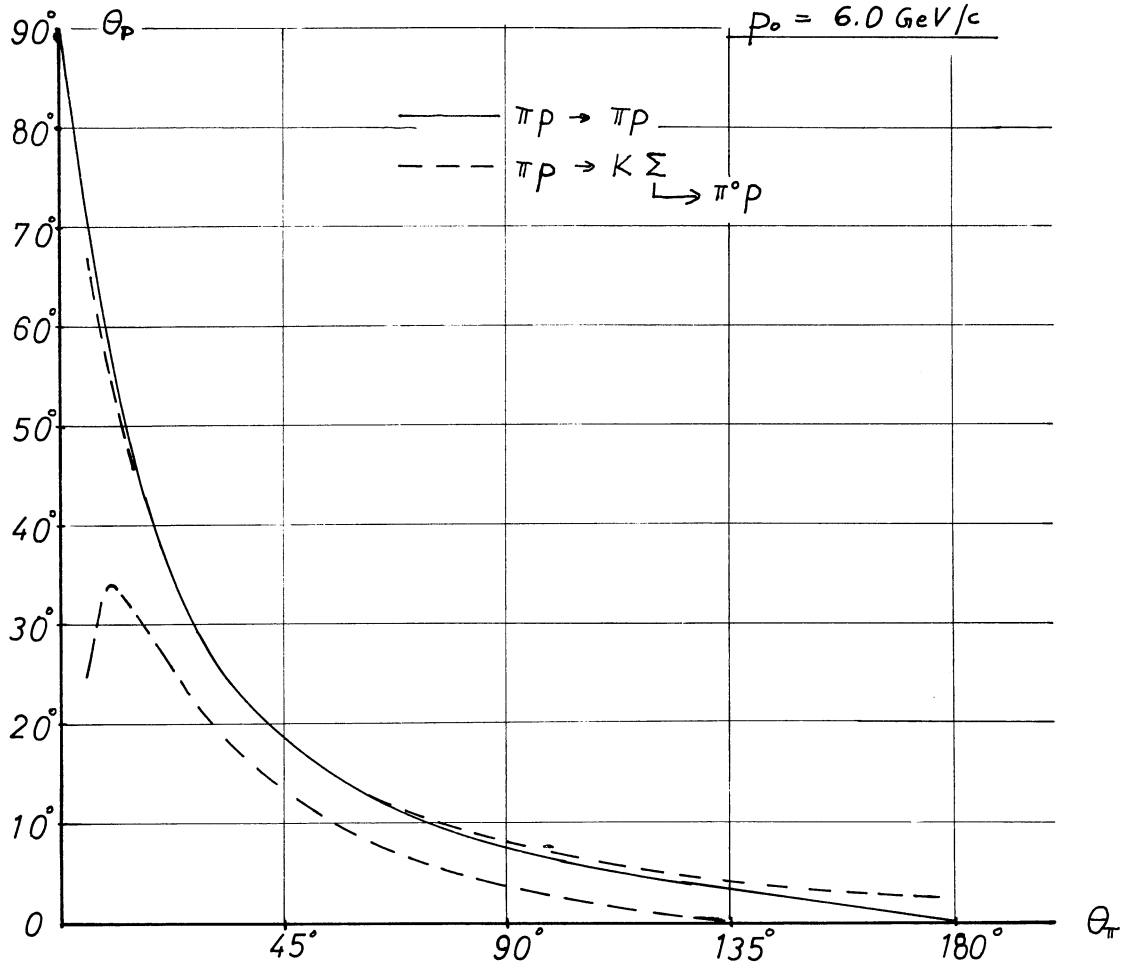

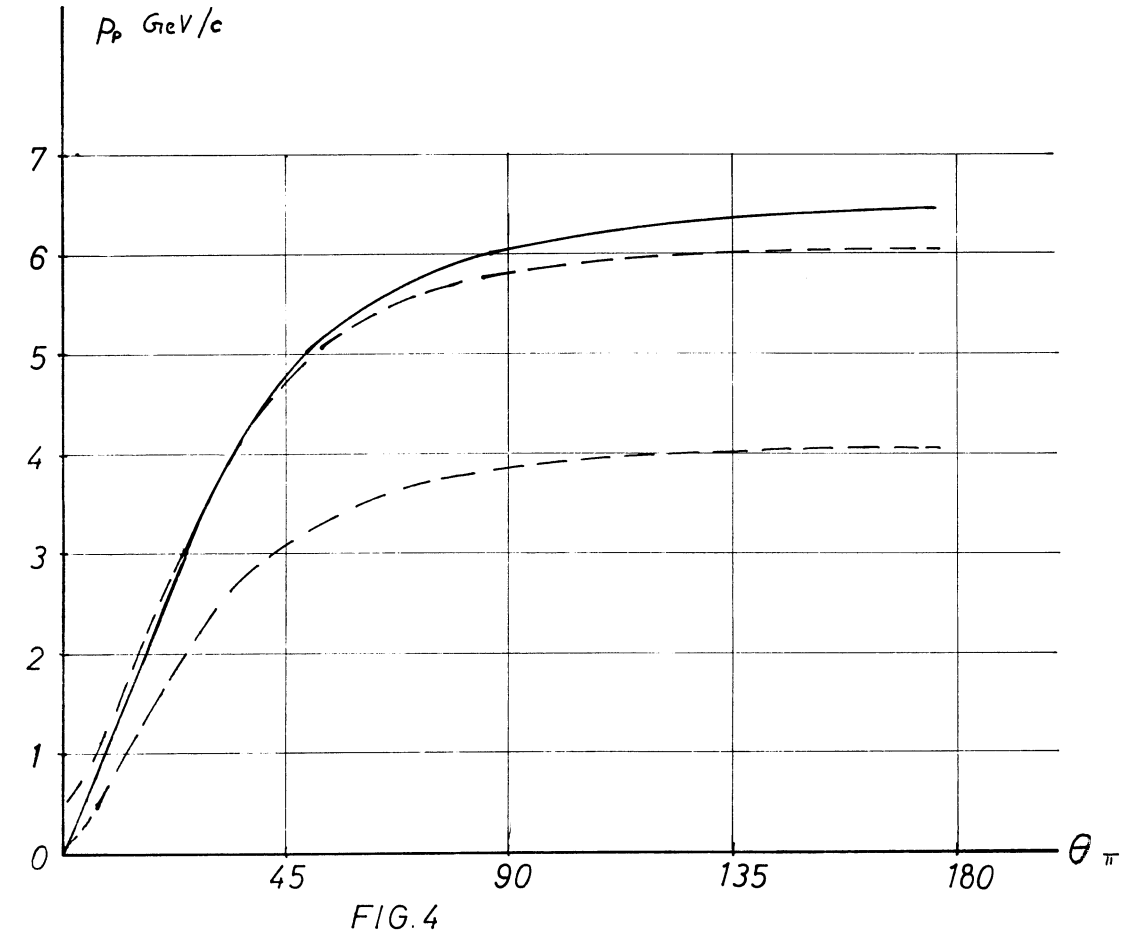

FIG. 4

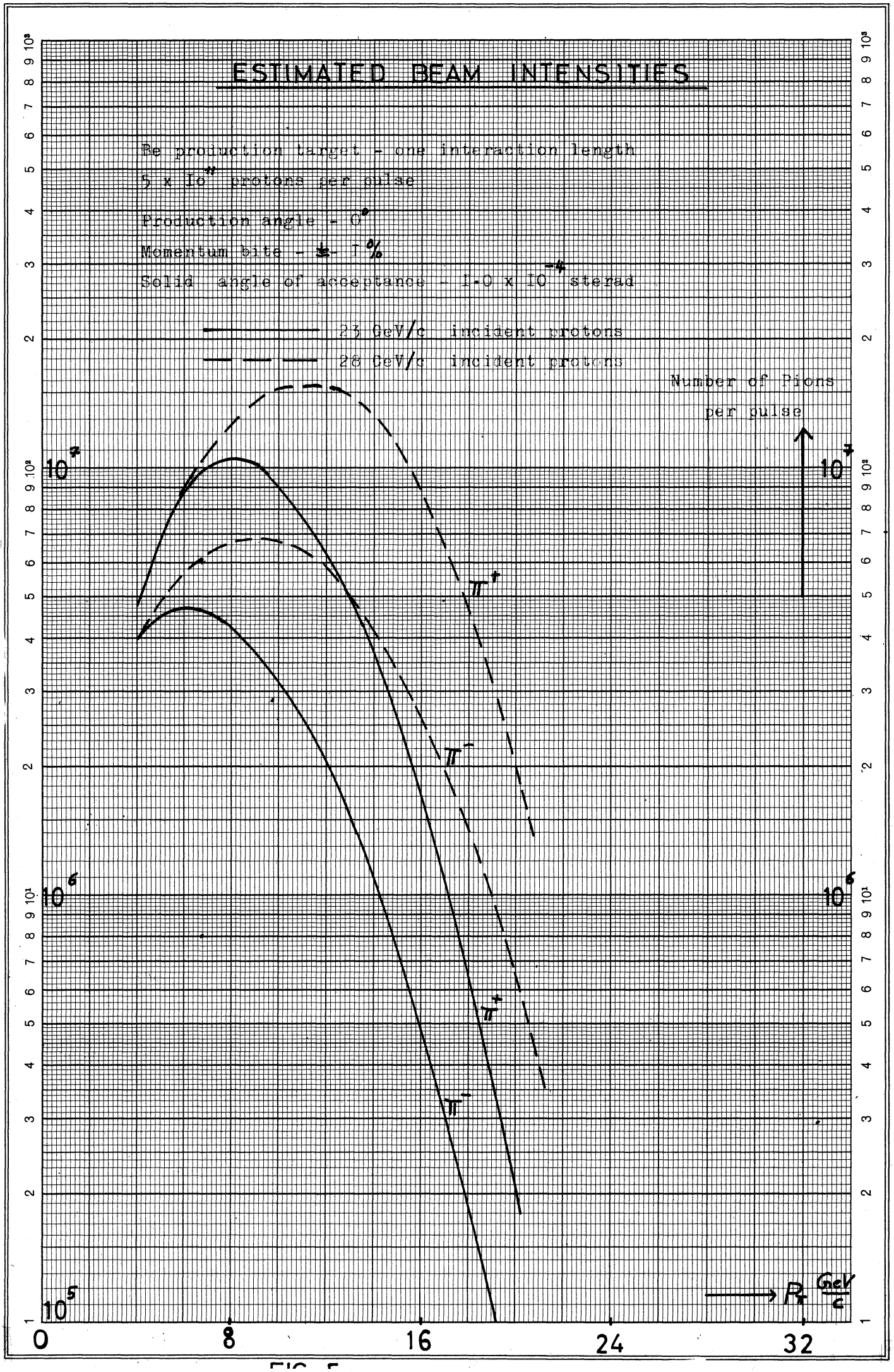

FIG. 5

SIS/R/12708

BEAM OPTICS

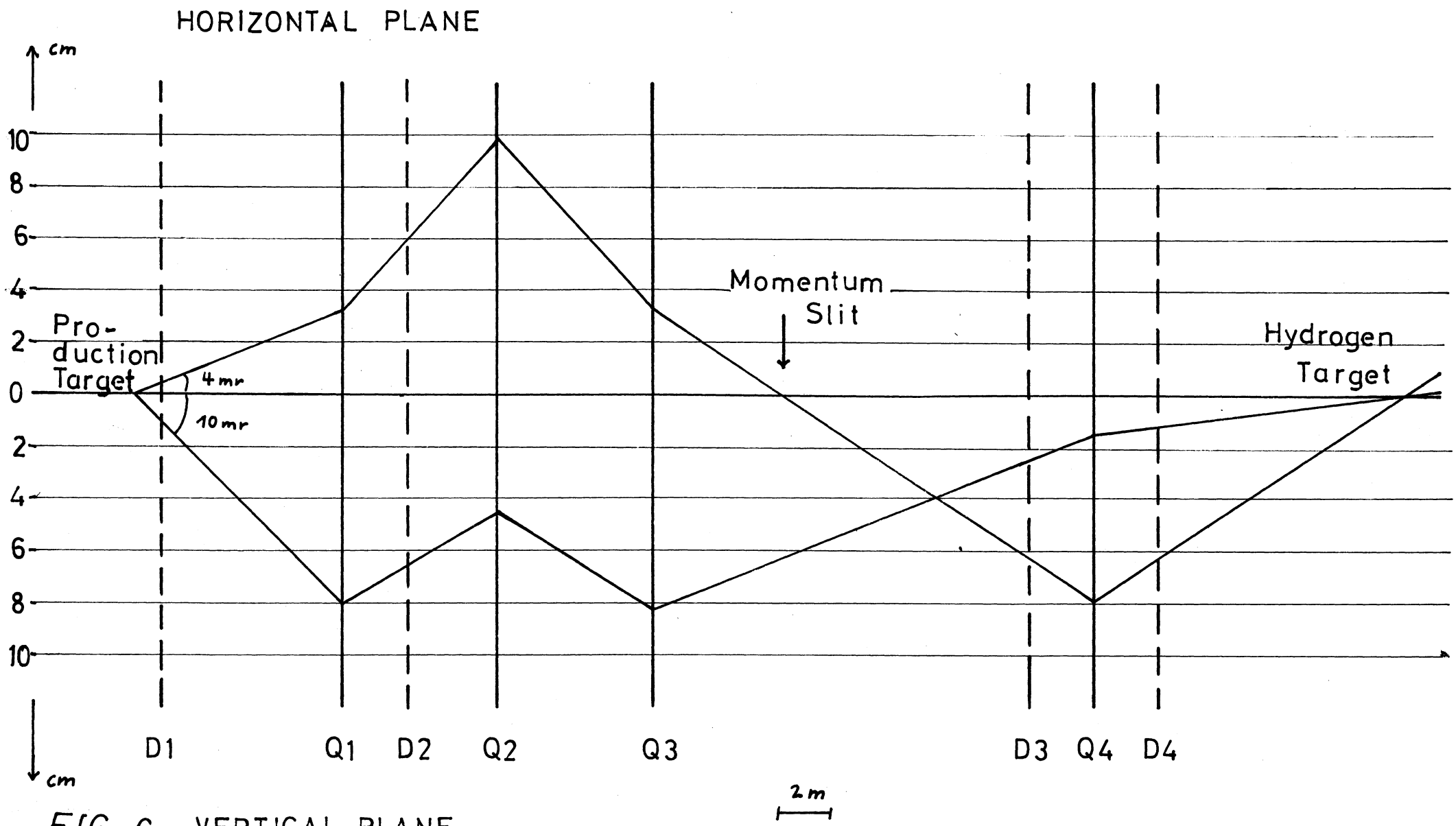

FIG. 6 VERTICAL PLANE

2m GAS ČERENKOV COUNTER

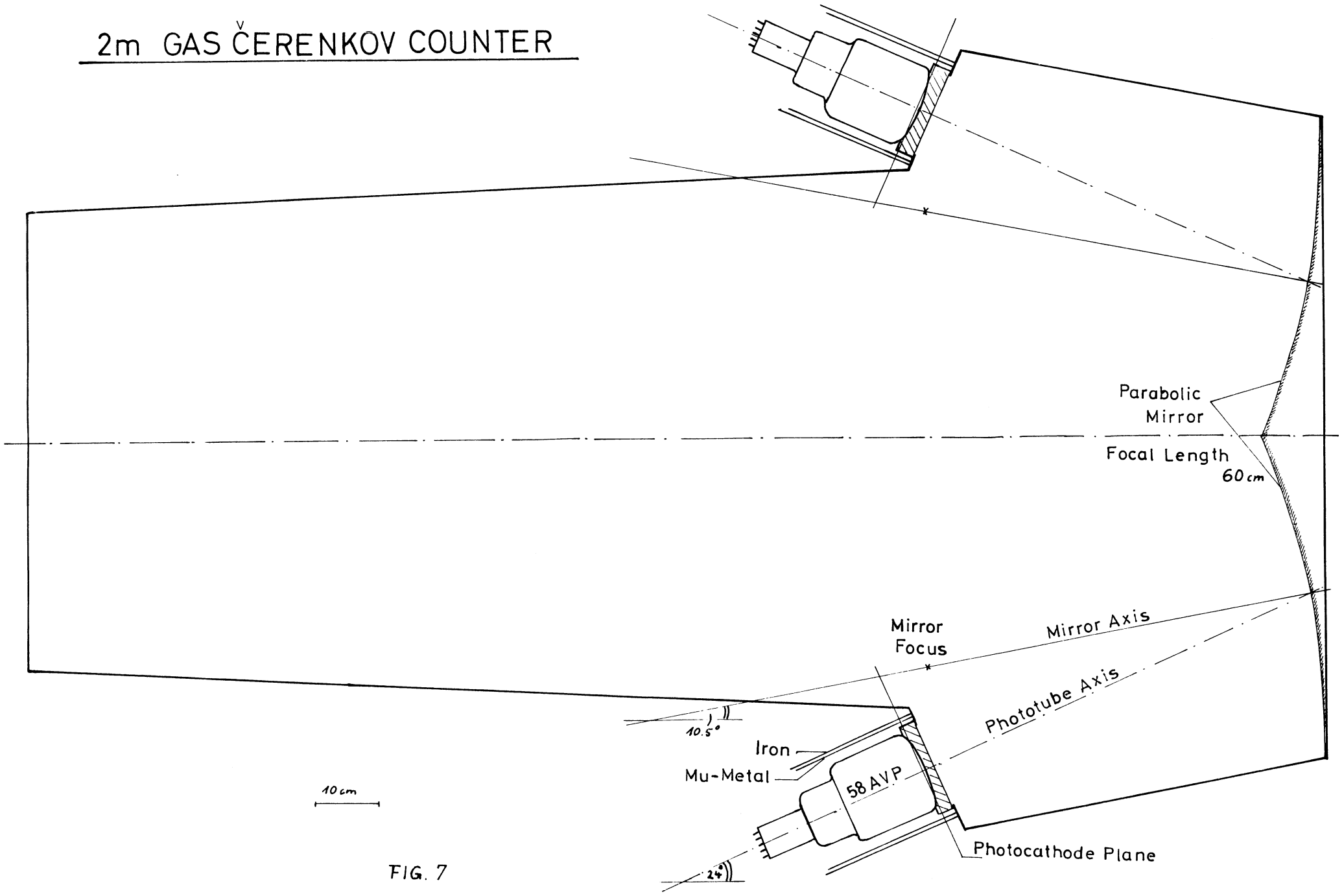

FIG. 7

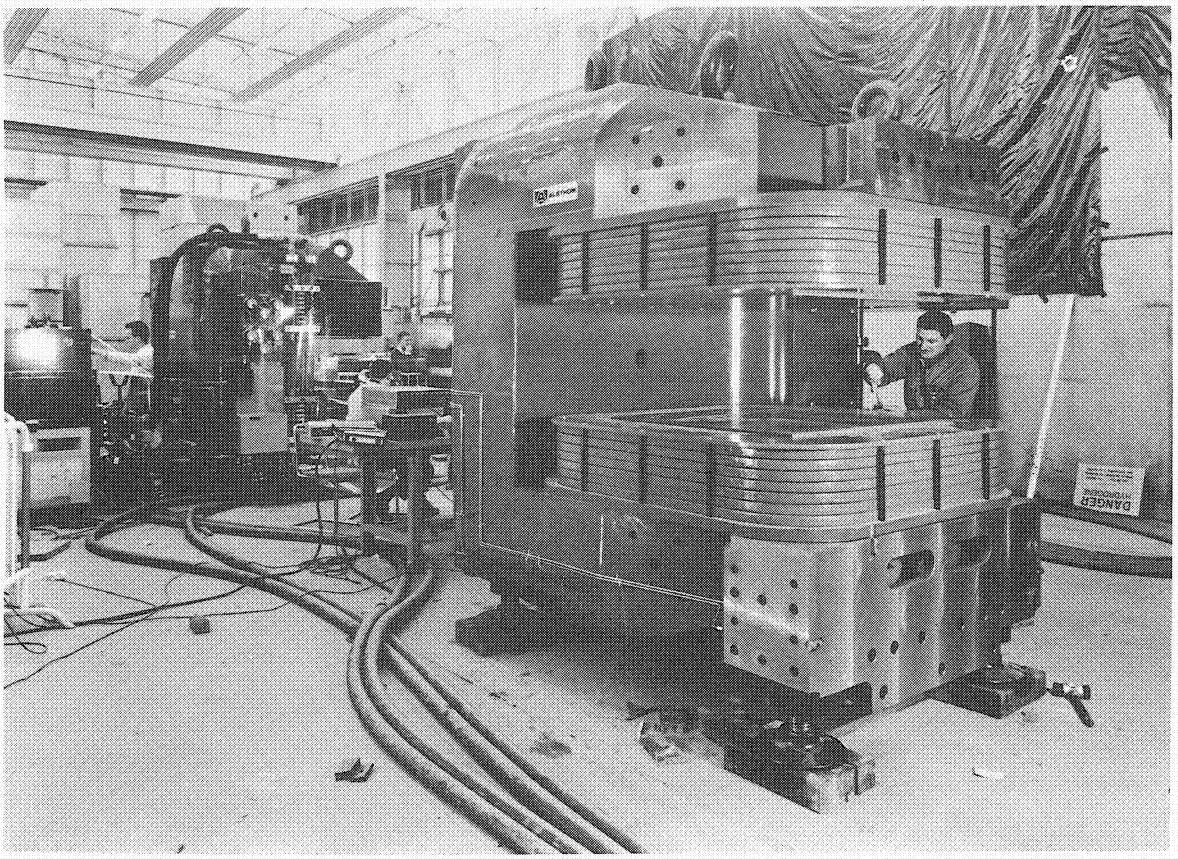

Fig. 8

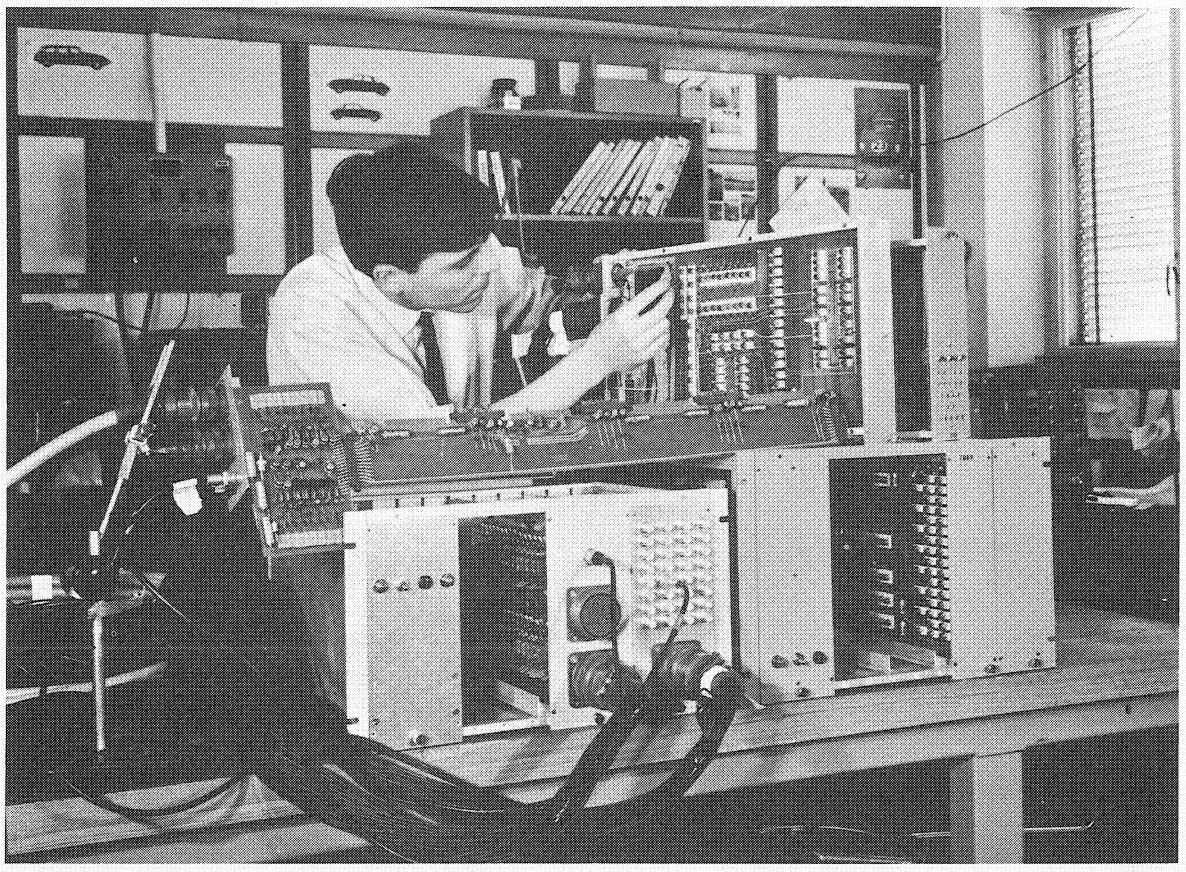

Fig. 9

DATA FLOW DIAGRAM

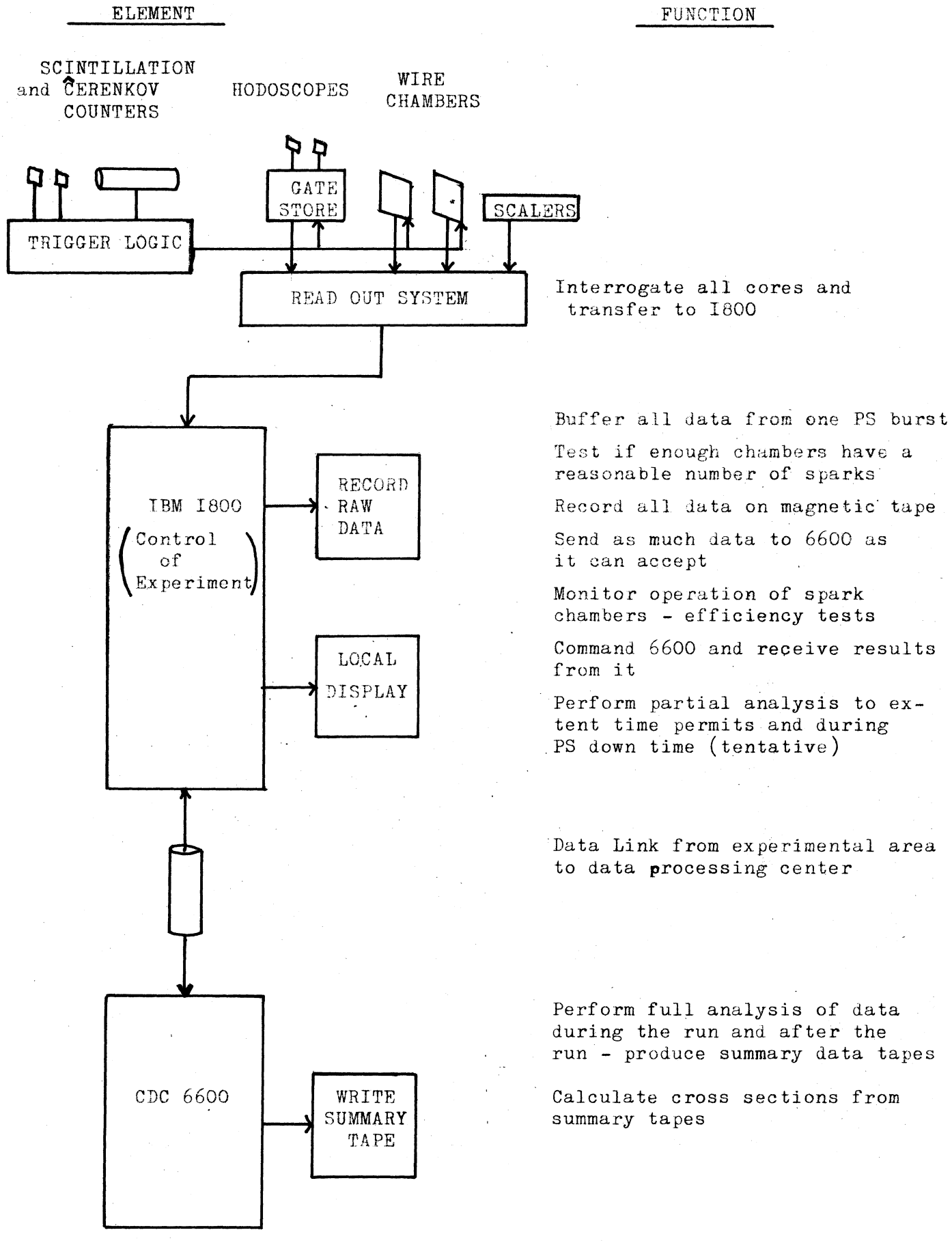

FIG. 10

SIS/R/12706

PROGRAM FLOW CHART

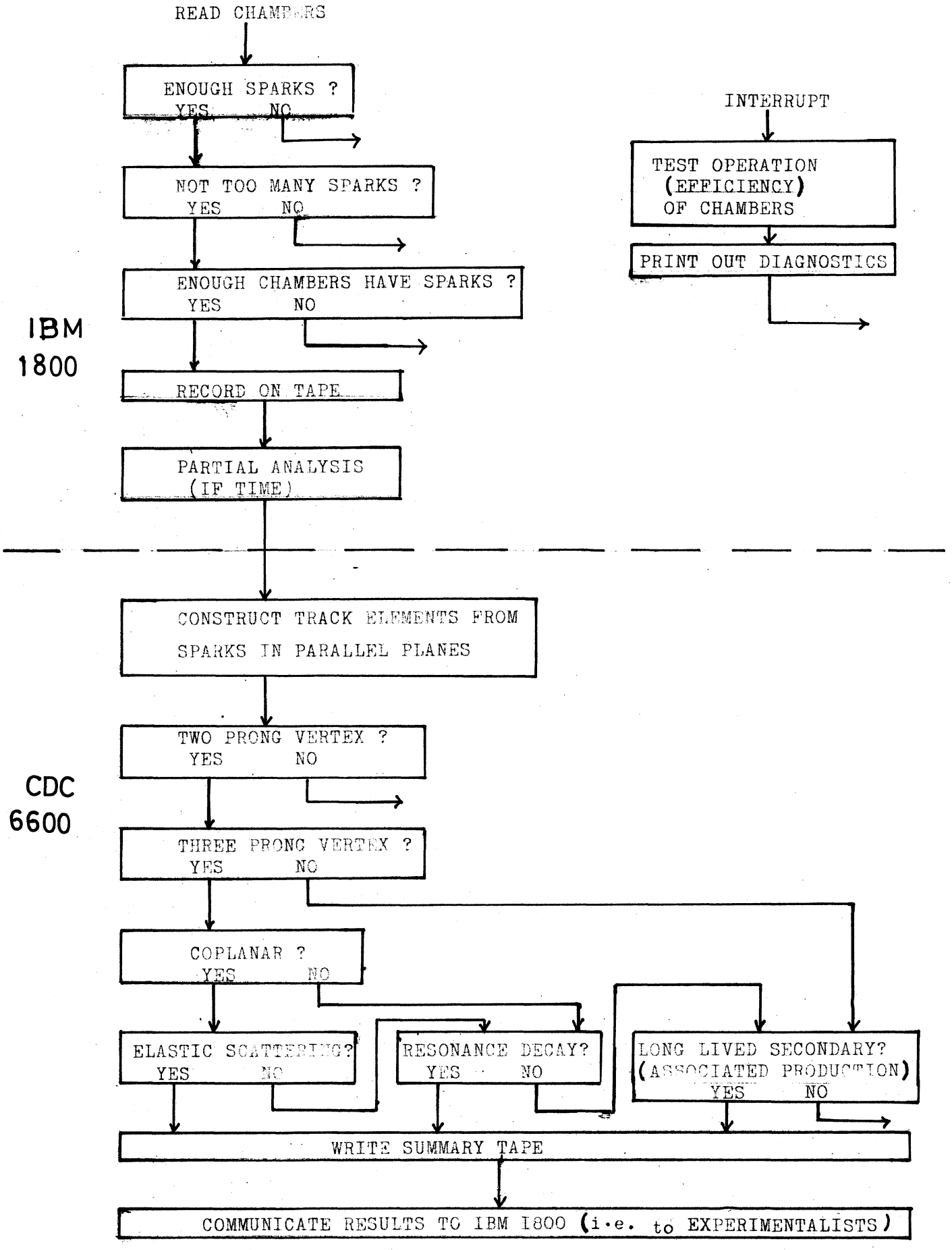

N.B. ON-LINE OPERATION ONLY IS SHOWN (↳ = go to next event)

SIS/R/12705

FIG. 11